Enhanced dimerization drives ligand-independent activity of mutant EGFR in lung cancer

Christopher C. Valley[1], Donna J. Arndt-Jovin[2], Narain Karedla[3], Mara P. Steinkamp[1], Alexey I. Chizhik[3], William S. Hlavacek[4], Bridget S. Wilson[1], Keith A. Lidke[5] and Diane S. Lidke[1]

Author affiliations:

[1]Department of Pathology and Cancer Research and Treatment Center, University of New Mexico, Albuquerque, NM, USA

[2]Laboratory of Cellular Dynamics, Max Planck Institute for Biophysical Chemistry, Göttingen, Germany

[3]III. Institute of Physics, Georg-August University of Göttingen, Göttingen, Germany

[4]Theoretical Biology and Biophysics Group, Theoretical Division, Los Alamos National Laboratory, Los Alamos, NM, USA

[5]Department of Physics and Astronomy, University of New Mexico, Albuquerque, NM, USA

Corresponding author: Diane Lidke, DLidke@salud.unm.edu

Running title: Kinase mutations drive EGFR dimerization

Abbreviations: EGFR – epidermal growth factor receptor; EGF – epidermal growth factor; RTK – receptor tyrosine kinase; NSCLC – Non-small cell lung carcinoma; QD – quantum dot; TKI – tyrosine kinase inhibitor; HMM – Hidden Markov Model; dSTORM – direct stochastic optical reconstruction microscopy; ACP – acyl carrier protein; FRET – Förster resonance energy transfer; FLIM – fluorescence lifetime imaging microscopy; HA – hemagglutinin tag

ABSTRACT

Mutations within the epidermal growth factor receptor (EGFR/erbB1/Her1) are often associated with tumorigenesis. In particular, a number of EGFR mutants that demonstrate ligand-independent signaling are common in non-small cell lung cancer (NSCLC), including kinase domain mutations L858R (also called L834R) and exon 19 deletions (e.g. ΔL747-P753insS) which collectively make up nearly 90% of mutations in NSCLC. The molecular mechanisms by which these mutations confer constitutive activity remain unresolved. Using multiple sub-diffraction-limit imaging modalities, we reveal the altered receptor structure and interaction kinetics of NSCLC-associated EGFR mutants. We applied two-color single quantum dot tracking to quantify receptor dimerization kinetics on living cells and show that, in contrast to wild type EGFR, mutants are capable of forming stable, ligand-independent dimers. Two-color super-resolution localization microscopy confirmed ligand-independent aggregation of EGFR mutants. Live cell FRET measurements revealed that the L858R kinase mutation alters ectodomain structure such that unliganded mutant EGFR adopts an extended, dimerization-competent conformation. Finally, mutation of the putative dimerization arm confirmed a critical role for ectodomain engagement in ligand-independent signaling. These data support a model in which dysregulated activity of NSCLC-associated kinase mutants is driven by coordinated interactions involving both the kinase and extracellular domains that lead to enhanced dimerization.

INTRODUCTION

The epidermal growth factor receptor (EGFR/erbB1/HER1) is a member of the erbB family of receptor tyrosine kinases (RTKs) that play a critical role in a number of physiological processes and are additionally implicated in the progression and prognosis of certain cancer types (Lemmon and Schlessinger, 2010). Additionally, EGFR is the target for numerous therapeutic strategies in such cancers, however patients often acquire resistance to such therapies. Therefore, there exists the need for novel approaches to targeting EGFR, which in turn requires the characterization of the structural and biophysical mechanisms by which EGFR signaling—both physiological and pathological—is initiated within the cell.

The current structural model of physiological EGFR activation includes ligand-induced, receptor-mediated dimerization of the ectodomain (Ogiso *et al.*, 2002; Schlessinger, 2002), which is propagated across the plasma membrane via interactions within the transmembrane (Arkhipov *et al.*, 2013; Endres *et al.*, 2013) and juxtamembrane domains (Thiel and Carpenter, 2007; Jura *et al.*, 2009; Red-Brewer *et al.*, 2009), resulting in allosteric activation of the kinase domain via asymmetric dimerization (Zhang *et al.*, 2006). Many aspects of this model, however, are based upon crystal structure or biochemical data of fragments of the entire protein. In such a system, any structural coupling (Lu *et al.*, 2010; Mi *et al.*, 2011) between various receptor domains is lost, as are the complexities involving the receptor interaction with the local environment (i.e. plasma membrane), which contribute both to receptor autoinhibition (Bremer *et al.*, 1986; McLaughlin *et al.*, 2005; Coskun *et al.*, 2011) and the stabilization of kinase activity (Mi *et al.*, 2008). Furthermore, many aspects of this model remain under debate, including ligand occupancy (Macdonald and Pike, 2008; Alvarado *et al.*, 2010), receptor structure/orientation (Kästner *et al.*, 2009; Kozer *et al.*, 2011; Tynan *et al.*, 2011), receptor oligomerization (Clayton *et al.*, 2005; Kozer *et al.*, 2013, 2014) , and receptor aggregation and supramolecular organization (Carraway *et al.*, 1989; Keating *et al.*, 2008; Abulrob *et al.*, 2010; Needham *et al.*, 2013, 2014). Therefore, there is an obvious need to study the structure of the receptor—including both receptor conformation and receptor interactions—within the plasma membrane environment.

Recent imaging technologies have captured EGFR behavior in living cells, providing quantitative measures of receptor interactions (Chung *et al.*, 2010; Low-Nam *et al.*, 2011; Valley *et al.*, 2014), phosphorylation (Sako *et al.*, 2000), and conformational states (Ziomkiewicz *et al.*, 2013). In previous work, we developed single molecule imaging techniques to visualize and quantify EGFR dynamics and dimerization on living cells (Lidke *et al.*, 2005; Low-Nam *et al.*, 2011). We showed that wild type EGFR dimers that form in the absence of ligand are short-lived and that receptor dimers are stabilized upon ligand binding (Low-Nam *et al.*, 2011). In other studies, Ziomkiewicz et al. used FRET measurements to study changes in EGFR ectodomain conformation and demonstrated ligand-induced structural rearrangements that are consistent with stabilization of the extended, dimer-competent conformation (Ziomkiewicz *et al.*, 2013). These results in live cells are consistent with dimerization being the initiating event in signal transduction, as predicted by structural and biochemical studies.

EGFR is often dysregulated in cancer by mutation or amplification. Specific mutations within the EGFR kinase domain are common in non-small cell lung cancer (NSCLC), including a somatic mutation resulting in a single amino acid substitution at leucine 858 to arginine (EGFR-L858R, or -L834R in the mature protein numbering) as well as in-frame deletions within exon 19 (e.g. EGFR-ΔL747-P753insS). Together, these mutations make up nearly 90% of EGFR-mutant NSCLC tumors (Sharma *et al.*, 2007; Pao and Chmielecki, 2010) and correlate with sensitivity to tyrosine kinase inhibitors (TKIs) (Lynch *et al.*, 2004; Paez *et al.*, 2004; Pao *et al.*, 2004). Expressed in model cells, EGFR kinase mutants, including EGFR-L858R and EGFR-ΔL747-P753insS, transform Ba/F3 and other cells via ligand-independent receptor activity at the cell surface and additionally confer sensitivity to TKIs (Greulich *et al.*, 2005; Jiang *et al.*, 2005; Choi *et al.*, 2007).

Although it is generally accepted that these NSCLC-associated mutations give rise to constitutive and unregulated activity, the precise molecular and biophysical mechanism(s) by which EGFR mutants initiate signaling from the plasma membrane remain unresolved. Crystal structures of the isolated EGFR-L858R kinase (Yun *et al.*, 2007) provided evidence that such activating mutations disrupt autoinhibitory interactions within the kinase, and this relief of autoinhibition leads to an increase in the activity of the purified, isolated kinase *in vitro* (Carey *et al.*, 2006; Zhang *et al.*, 2006; Yun *et al.*, 2007). Further studies demonstrated a clear requirement for asymmetric kinase dimerization of certain NSCLC-associated EGFR mutants, including

L858R (Cho *et al.*, 2013), which preferentially adopts the receiver conformation within the asymmetric kinase dimer (Red-Brewer *et al.*, 2013) by suppressing local disorder within the N-lobe region of the kinase dimer interface (Shan *et al.*, 2012).

While it is plausible, if not probable, that such mutations which shift the equilibrium of the kinase domain to the active conformation will promote kinase dimerization, it remains unknown whether such a driving force is sufficient to facilitate dimerization of the full length receptor. Recent work using purified, near full-length EGFR demonstrated that NSCLC kinase mutant L858R readily dimerizes in the absence of ligand (Wang *et al.*, 2011). However, the plasma membrane is known to play a critical role in the negative regulation of EGFR (Bremer *et al.*, 1986; McLaughlin *et al.*, 2005; Coskun *et al.*, 2011) and likely dictates conformational coupling between various receptor domains, evident from the altered ligand binding and functional stability depending on the local environment (Mi *et al.*, 2008; Wang *et al.*, 2011).

Here, using multiple sub-diffraction-limit imaging modalities, we reveal the altered behavior of NSCLC-associated EGFR mutants in living cells. We directly show that NSCLC-mutant EGFR form stable dimers even in the absence of ligand and that unliganded mutant EGFR adopts an extended, dimerization-competent conformation. Furthermore, we demonstrate that, while the NSCLC-associated mutations are located in the kinase domain, ectodomain interactions via the well-characterized dimerization arm are necessary for efficient ligand-independent activity. Collectively, these results show that dysregulated activity of NSCLC-associated kinase mutants is driven by coordinated interactions involving multiple receptor domains that lead to enhanced dimerization.

RESULTS

Ligand-independent phosphorylation of NSCLC-associated EGFR mutants is highly dependent on receptor density in the membrane. We stably expressed EGFR with an N-terminal HA-tag (HA-EGFR) in CHO cells, which lack endogenous EGFR. Transfected cells expressed either the wild type EGFR (EGFR-WT), EGFR-L858R, or EGFR-ΔL747-P753insS.

Figure 1 compares the levels of EGFR phosphorylation on tyrosine 1068. In contrast to the WT receptor, expression of EGFR-L858R or EGFR-ΔL747-P753insS resulted in measurable receptor phosphorylation in the absence of ligand (Figure 1A). As previously reported (Choi *et al.*, 2007), both mutant forms of EGFR retain the capacity for ligand-induced activation as measured by receptor phosphorylation, albeit reduced compared to EGFR-WT. Sensitivity to the EGFR-selective inhibitor PD153035 (Bos *et al.*, 1997) is consistent with receptor phosphorylation independent of endogenous kinases in CHO cells (Figure 1A).

As expected for a stable cell line, expression of EGFR is heterogeneous in transfected CHO cells. Confocal imaging of cells double-labeled with pan-reactive EGFR antibodies (anti-HA) and phospho-specific antibodies (anti-pY1068) revealed the relationships between local EGFR expression level and phosphorylation state (Figure 1B). In the absence of ligand, EGFR-WT exhibits barely measurable phosphorylation of tyrosine 1068 (Figure 1B). In contrast, results for the cells expressing mutant EGFR show significant levels of phosphorylation. Control responses in the presence of ligand are consistent with western blotting results (Figure S1). Quantification of these images confirmed that the NSCLC mutants show a robust, ligand-independent phosphorylation response with the level of overall receptor phosphorylation dependent on increasing receptor expression (Figure 1C).

Considering the two possible mechanisms for increased ligand-independent phosphorylation of EGFR mutants, and to determine if one mechanism might dominate, we fit the data in Figure 1C to a monomer-dimer equilibrium model assuming either (*i)* higher intrinsic kinase activity (Zhang *et al.*, 2006; Yun *et al.*, 2007) (See Supplementary Note, Table S3 - Model 1) or *(ii)* increased dimerization affinity (Shan *et al.*, 2012) (See Supplementary Note, Table S3 - Model 2). As shown Figure 1C, however, both models yielded equal goodness of fit (compare the solid and dashed curves, see also Figure S2). We also used computational modeling to explore alternative mechanisms of EGFR dimerization, including dimerization via multiple ectodomain conformations and both ectodomain- and endodomain-mediated interactions, and found that such mechanisms yield the same functional relationship between EGFR abundance and EGFR phosphorylation (see Supplementary Note for a detailed description of all models). Therefore, both augmented kinase activity and altered dimerization sufficiently describe the data, and further experiments were needed to delineate the contribution of either mechanism. Given that EGFR-WT activation is driven by ligand-induced dimerization (Burgess *et al.*, 2003; Chung

et al., 2010; Low-Nam *et al.*, 2011), and mutant activity relies on asymmetric kinase dimerization (Cho *et al.*, 2013; Red-Brewer *et al.*, 2013), we tested the strong possibility that NSCLC mutations enhance ligand-independent receptor dimerization.

EGFR kinase mutations facilitate receptor dimerization and decrease receptor mobility in the native plasma membrane. We applied two-color SPT methods to directly visualize and quantify EGFR diffusion and dimerization in live cells (Lidke *et al.*, 2005; Low-Nam *et al.*, 2011; Steinkamp *et al.*, 2014). Receptors were tracked using spectrally distinct quantum dots (QDs), QD585 and QD655, conjugated to either EGF (Lidke *et al.*, 2004; Low-Nam *et al.*, 2011) or a monovalent anti-HA Fab fragment (Steinkamp *et al.*, 2014); these probes track the liganded and unliganded receptor, respectively. QDs are robust SPT probes that provide high brightness and photostability, without impairing the diffusion properties or physiological response of membrane receptors (Dahan *et al.*, 2003; Lidke *et al.*, 2004; Chung *et al.*, 2010; Low-Nam *et al.*, 2011; Schwartz *et al.*, 2015). Dimer events are imaged by independent localization of single molecules in the two spectral channels with high spatial (~20 nm) and temporal (50 ms) resolution (Low-Nam *et al.*, 2011). As shown schematically in Figure 2A, combinations of these probes enabled the tracking of different dimer species: unliganded dimers (0-EGF:2-EGFR), ligand-bound dimers (2-EGF:2-EGFR), and singly-liganded dimers (1-EGF:2-EGFR). Critically, labeling of EGFR with anti-HA-QDs did not cause activation of the receptor in the absence of EGF, nor did it prevent receptor activity or dimerization in the presence of saturating dark EGF (Figure S3).

Figure 2B-D shows examples of repeated dimerization events between receptor pairs with varying dimer stability. The unliganded EGFR-WT exhibited transient dimers (Figure 2B and Movie S1), whereas the ligand-bound EGFR-WT formed longer-lived dimers (Figure 2C and Movie S2). In contrast to EGFR-WT, both mutants demonstrated long-lived interactions in the absence of ligand (Figure 2D and Figure S4; Movie S3 and S4). Dimerization kinetics were estimated using a three-state Hidden Markov Model (HMM) as previously described (Low-Nam *et al.*, 2011). The HMM utilizes the distance between two spectrally distinct QDs as the experimental observable and globally fits all the data in a single condition using a maximum likelihood estimation to extract the rate constants for transitions between dimer and non-dimer

(i.e. hidden) states. Therefore, while the labeled receptors may be undergoing interactions with unlabeled proteins, the off-rates are only calculated from observed two-color dimerization events. Based on calculated transition rates, the Viterbi algorithm can be used to identify the dimerization state for a pair of receptors at each point within a time series (Figure 2B-D, lower panel). The resulting dimer off-rates calculated over many dimer interactions are shown in Figure 2E and summarized in Table S1. Consistent with our previous work (Low-Nam *et al.*, 2011), EGFR-WT receptors formed short-lived dimers in the absence of ligand (dimer off-rate, $k_{off} = 0.31\ s^{-1}$) that shifted to longer-lived dimers with ligand bound ($k_{off} = 0.12\ s^{-1}$). The singly-liganded EGFR-WT dimer had an intermediate off-rate. While others have reported EGF unbinding rates on the order of our measurement time, but much longer than our dimer lifetime (Hendriks *et al.*, 2003; Mattoon *et al.*, 2004), we have not observed significant losses of EGF-QD during our time courses. Even though this could lead to a small underestimate of the dimer off-rate, the interpretation of the relative differences between conditions is unaffected. Importantly, homodimers composed of EGFR-L858R or EGFR-ΔL747-P753insS mutants were stable regardless of ligand occupancy, with off-rates similar to ligand-bound EGFR-WT (Figure 2E). These results indicate that kinase mutations drive the formation of stable dimers in the absence of EGF.

Our previous studies showed that EGF-bound EGFR forms stable dimers that exhibit markedly reduced mobility (Low-Nam *et al.*, 2011). We found that the EGFR mutants, both in the presence and absence of ligand, displayed mobility more similar to ligand-bound EGFR-WT (Figure 2F). Receptor mobility was quantified by calculating the distribution of squared displacements and is shown as a cumulative probability plot in Figure 2G. As expected, a significant shift to slower mobility is seen for ligand-bound EGFR-WT. Decreased mobility is dependent on receptor phosphorylation and reflects the complexities of signaling-mediated changes, such as recruitment of downstream proteins and changes in the local membrane environment. The EGFR mutants exhibited a similar reduction in mobility, even in the absence of ligand. The average diffusion coefficients are given in Figure 2H (see also Table S1). Upon ligand binding, both mutants slowed further to a degree comparable to that of ligand-bound EGFR-WT, consistent with a further increase in receptor interactions driven by ligand binding. We interpret the reduced mobility of unliganded mutant receptors to be a function of their increased number of dimer events, as well as the recruitment of signaling proteins.

Two-color super-resolution microscopy confirms ligand-induced EGFR aggregation and ligand-independent EGFR mutant aggregation. To further support the conclusion that EGFR-L858R and EGFR-ΔL747-P753insS mutants dimerize more readily than EGFR-WT, we used two-color direct stochastic optical reconstruction microscopy (dSTORM) (Heilemann *et al.*, 2008) to visualize the distribution of EGFR in the plasma membrane (Figure 3A, B). Receptor proximity across multiple samples was quantified using localization-based cross-correlation analysis of Alexa647- and Cy3B-labeled EGFR. As plotted in Figure 3C, the correlation function for unliganded EGFR-WT is ~1 across all distances, indicating a nearly random distribution of receptors in the plasma membrane.

In contrast to the near random distribution of resting EGFR, stimulation with saturating EGF induced a strong peak below 50 nm in the correlation function, indicating clustering of receptors at short distances that is consistent with the conventional model for ligand-induced dimerization (Schlessinger, 2002; Burgess *et al.*, 2003). Analysis of reconstructed images for EGFR-L858R or EGFR-ΔL747-P753insS without EGF addition are shown in Figure 3D. An increase in the correlation function at short distances (< 50 nm) was seen for both mutants, providing further evidence for increased self-association of EGFR mutants in the absence of ligand (Figure 3D). Cross-correlation values for EGFR-L858R within the dimerization-permissive distance were higher than for EGFR-ΔL747-P753insS, consistent with modeling predictions reported in Figure 1C for a lower relative K_D (see Tables S3 and S4).

Activating kinase mutations alter the ectodomain structure. Prior studies using recombinant EGFR kinase domain has shown that NSCLC-associated EGFR mutant kinases exhibit increased catalytic activity (Zhang *et al.*, 2006), possibly by adopting an active conformation (Shan *et al.*, 2012). Our studies of full-length receptors in intact cells have indicated an additional property of both EGFR-L858R and EGFR-ΔL747-P753insS mutations: they promote the formation of stable homodimers within the plasma membrane of live cells in the absence of ligand. Thus, our observations imply that the EGFR kinase domain mutations induce structural changes that facilitate receptor dimerization.

To test this hypothesis, we monitored the conformational states of the EGFR ectodomain via FRET measurements in living cells using fluorescence lifetime imaging microscopy (FLIM) (Ziomkiewicz *et al.*, 2013), shown schematically in Figure 4A. EGFR-WT and EGFR-L858R were generated with N-terminal acyl carrier protein (ACP) tags and expressed in CHO cells. The ACP-tag was coupled to a small FRET donor, Oregon Green, through the covalent attachment of labeled-CoA. Cells were subsequently labeled with the FRET acceptor, NR12S, a lipid probe that is retained in the outer leaflet of the plasma membrane (Kucherak *et al.*, 2010) (Figure S5). The extent of energy transfer between the EGFR donor tag and lipid acceptor, was determined by monitoring the donor fluorescence lifetime under various conditions (Figure 4B-D, Table S2). As shown previously (Ziomkiewicz *et al.*, 2013), EGFR-WT exhibited a shorter donor lifetime (corresponding to high energy transfer) in the absence of ligand (3.14 ± 0.05 ns), which significantly increased upon EGF addition (3.37 ± 0.05 ns) (Figure 4D, blue). This reduction in FRET with EGF addition is consistent with ligand-induced extension of the extracellular domain away from the plasma membrane (Burgess *et al.*, 2003; Ziomkiewicz *et al.*, 2013) (Figure S6), in contrast to previously proposed models (Webb *et al.*, 2008; Kästner *et al.*, 2009; Tynan *et al.*, 2011). Interestingly, we observed a longer donor lifetime (lower FRET efficiency) for EGFR-L858R in the absence of ligand (3.34 ± 0.03 ns) relative to unliganded EGFR-WT (Figure 4D, red), suggesting a bias in ectodomain structure in the kinase mutant favoring the extended, dimer-competent conformation. We note that the further increase in lifetime for EGFR-L858R upon EGF addition (3.53 ± 0.04 ns) is consistent with ligand-induced activity (Figure 1A) and an increased ligand-binding affinity (Choi *et al.*, 2007), however the relationship between structure and affinity is not fully understood (Mattoon *et al.*, 2004).

Ectodomain engagement is required for robust, ligand-independent signaling of EGFR-L858R. To understand whether ectodomain interactions were indeed required for ligand-independent activity of EGFR-L858R, we introduced a series of mutations to amino acids within the dimerization arm (246-253*) that are critical for receptor dimerization and activity (Dawson *et al.*, 2005) and expressed these mutants in HeLa cells. As predicted based on these biochemical studies, mutation of the dimerization arm resulted in no change in EGFR-WT mobility upon the addition of saturating EGF (Figure S7) indicating that ectodomain dimerization is indispensable for ligand-induced activity. Consistent with results in CHO cells (Figure 1-2), EGFR-L858R

shows ligand-independent phosphorylation and exhibits decreased mobility relative to EGFR-WT (Figure 5). We found that EGFR-L858R/246-253*, containing both an activating kinase mutation and mutation of the ectodomain dimerization arm, had significantly diminished ligand-independent phosphorylation (Figure 5A-B, Figure S8) and also increased mobility relative to EGFR-L858R kinase mutant alone (Figure 5C-D). The doubly mutated EGFR-L858R/246-253* retained measurable levels of ligand-independent activity compared to the EGFR-WT (Figure 5A, B). These results confirm a critical role for ectodomain engagement via interactions in the dimerization arm in the ligand-independent signaling of intracellular kinase mutants associated with NSCLC.

DISCUSSION

In this study, we have applied complimentary high-resolution imaging techniques to better understand the molecular mechanisms underlying the aberrant activity of EGFR NSCLC mutants. We show that NSCLC mutations facilitate ligand-independent receptor dimerization. Our results additionally reveal that the mechanism of signal initiation for the kinase domain L858R mutant involves ectodomain interactions via the dimerization arm, stabilizing the receptor in the extended, dimer-competent conformation. Therefore, our data support the hypothesis that oncogenic signaling from these NSCLC-associated EGFR mutants occurs as a result of enhanced, productive dimerization between unliganded receptors.

Several studies have demonstrated that asymmetric kinase dimerization is required for the ligand-independent activity of NSCLC-associated EGFR kinase mutants (Cho *et al.,* 2013; Red-Brewer *et al.,* 2013). Crystal structures showed that such mutations shift the equilibrium of the kinase domain toward an active conformation (Yun *et al.*, 2007), and recent studies demonstrated that this occurs by suppressing intrinsic disorder within the kinase domain N-lobe (Shan *et al.,* 2012), allowing the mutant kinase domains to act as "super-acceptors" within an asymmetric kinase dimer (Red-Brewer *et al.,* 2013). Interestingly, other mutations, such as exon 19 deletion and exon 20 insertions, are active as either activator or receiver (Cho *et al.*, 2013). Given this result, an important consideration is the interaction between NSCLC EGFR variants and either

the wild type EGFR or erbB2. It has been reported that patients with L858R mutation or exon 19 deletions are heterozygous (Lynch *et al.*, 2004), suggesting that oncogenic, pro-survival is a result of signaling via one mutant and one wild type EGFR. Our results in CHO cells, which lack endogenous EGFR-WT, and in HeLa cells, which have endogenous EGFR-WT, are consistent, indicating that EGFR-WT:EGFR-L858R kinase interactions do not overcome the need for ectodomain engagement. Further work is needed to determine whether the EGFR-WT:EGFR-L858R or erbB2:EGFR-L858R heterodimers form stable interactions as do to the L858R and exon 19 deletion receptor homodimer species studied here. Nevertheless, in the context of our results, it is clear that the function of NSCLC kinase mutants is dependent on dimerization via coordinated interactions both in the kinase domain and ectodomain.

The influence of the kinase domain mutations on extracellular domain behavior would suggest a structural coupling between the two domains. The relationship between the structure of the intracellular and extracellular domains of EGFR remains largely controversial (Bessman and Lemmon, 2012). There is experimental evidence for a well-defined structural linkage between intracellular and extracellular domains, where alterations to intracellular regions, including the juxtamembrane and kinase domains, influence extracellular ligand binding properties of the receptor (Choi *et al.*, 2007; Macdonald and Pike, 2008; Alvarado *et al.*, 2010). If these domains are rigidly linked, activating mutations in the kinase domain may drive extension of the ectodomain independent of kinase interactions. Alternatively, recent results show remarkable flexibility between intracellular and extracellular domains. Using disulfide cross-linking in cells as well as negative-stain EM of purified, near full-length EGFR (tEGFR), Lu et al. provided evidence that receptor dimerization can be driven through the kinase domain when it is stabilized in the active conformation. These results showed a high degree of structural variability in the ectodomain and no contacts in the dimerization arm domain compared to that of EGF-mediated dimers (Lu *et al.*, 2012). In an additional study, simultaneous visualization of extracellular and intracellular domains of tEGFR in the presence of Gefitinib, an EGFR-specific tyrosine kinase inhibitor which stabilizes the active and dimeric kinase domain, suggests a range of ectodomain conformations and little conformational coupling between these domains (Mi *et al.*, 2011). In the case that the intracellular and extracellular domains are flexibly linked, ligand-independent activity of NSCLC mutants would conceivably be initiated via kinase domain dimerization and stabilized by subsequent interactions within the ectodomain.

While our results cannot distinguish between these mechanisms of dimerization, we have shown that ectodomain engagement through the dimerization arm is required for optimal ligand-independent signaling of EGFR kinase mutants. It is conceivable that such a structural linkage exists in the wild type receptor, and, considering that the ensemble of structural states exist in equilibrium, constitutive activity of overexpressed EGFR-WT may be explained by an increased probability for productive receptor encounters, leading to ligand-independent dimerization (Martin-Fernandez *et al.*, 2002; Lidke *et al.*, 2003; Nagy *et al.*, 2010; Endres *et al.*, 2013). Interestingly, mutation of the dimerization arm does not completely abolish phosphorylation of EGFR-L858R (Figure 5A-B), indicating that kinase domain dimerization alone, while perhaps less stable in the absence of ectodomain engagement, can still produce some level of ligand-independent signaling. This dominating influence of the ectodomain in dimer stabilization is consistent with the ability of ligand-bound EGFR to form dimers when the kinase domain is either inhibited or removed (Chung *et al.*, 2010; Low-Nam *et al.*, 2011).

We have discussed EGFR signal initiation primarily in the context of dimerization as a result of extended ectodomain conformation (Burgess *et al.*, 2003), which is stabilized by ligand binding or mutation. However, we acknowledge the existence of alternative models for EGFR activation. For example, some studies have suggested that the presence of preformed dimers in the absence of EGF that transition to tetramers upon EGF binding (Clayton *et al.*, 2005). Other studies have indicated alternative ectodomain structures, including evidence that the EGFR ectodomain exists in an extended conformation in the cell membrane independent of ligand status (Kozer *et al.*, 2011) or that liganded receptor or preformed dimer collapses on the plasma membrane (Tynan *et al.*, 2011; Arkhipov *et al.*, 2013). Here, we have confirmed that while wild type receptor interactions in the absence of ligand can occur, they are short-lived (Figure 2B). Furthermore, quantitative analysis of super-resolution data showed a nearly random distribution of unliganded EGFR-WT (Figure 3), indicating predominantly monomeric receptor in the absence of ligand. These results are not consistent with preformed dimers as the predominant species in the absence of ligand. Our results are consistent with a monomer-dimer transition driving signaling. Receptor interactions are longer-lived in the presence of EGF (Figure 2C, Figure 3C) or by mutation to an active kinase domain (Figure 2D and Figure 3D). Furthermore, on the basis of live cell FRET data, the relatively long lived interactions of liganded or mutated receptors are associated with greater occupancy of the ectodomain extended conformation

(Figure 4 and (Ziomkiewicz *et al.*, 2013)). Recent MD simulations of the full-length, glycosolated receptor in a complex lipid environment lend support for our live cell FRET by demonstrating that glycosolation prevents such a collapsed receptor conformation (Kaszuba *et al.*, 2015). We note that many of the apparent inconsistencies between studies may be explained by experimental variations such as use of fixed cells, non-physiological temperatures, pharmacological inhibitors, or steric hindrance due to labeling. While our live cell data supports the model of dimers as the fundamental signaling unit, we cannot rule out a potential role for higher-order oligomers.

Our result that dimerization arm interactions are critical for robust ligand-independent signaling of the NSCLC-associated L858R mutant (Figure 5) suggests that targeting the ectodomain for EGFR-L858R, may inhibit the ligand-independent activity of these mutants. Such targeting molecules could include antibodies against the EGFR ectodomain (Li *et al.*, 2008; Rivera *et al.*, 2008; Schmiedel *et al.*, 2008; Talavera *et al.*, 2009) or peptides which disrupt EGFR dimerization arm-mediated interactions (Hanold *et al.*, 2015a, 2015b). Cetuximab is a potent inhibitor of EGFR activity and functions by both blocking ligand binding and by preventing the receptor from adopting the extended conformation (Li *et al.*, 2005). Several studies have used Cetuximab to block activity of NSCLC EGFR mutants with varying results (Wang *et al.*, 2011; Cho *et al.*, 2013).

The results presented here provide a biophysical basis for signal initiation in specific mutations associated with NSCLC. However, it remains unknown whether this mechanism of activation—including ectodomain engagement—is required in other variants of EGFR. The EGFRvIII variant, commonly found in glioblastomas (Gan *et al.*, 2009), lacks key residues in the ectodomain—including the dimerization arm—and therefore circumvents the need for dimerization arm engagement. The acquisition of a secondary, "gatekeeper" mutation within the EGFR kinase domain (T790M) renders patients insensitive to clinical TKIs (Kobayashi *et al.*, 2005; Pao *et al.*, 2005; Godin-Heymann *et al.*, 2008). Previous results suggested ligand-independent activity EGFR-L858R/T790M expressed in Ba/F3 cells was dimerization-independent based on resistance to Cetuximab (Cho *et al.*, 2013). The increased affinity for ATP of EGFR-L858R/T790M (Yun *et al.*, 2008) may accelerate receptor phosphorylation and

effectively circumvent the requirement for stable dimer formation, however this remains unknown.

In summary, this work provides critical new insight into the structural and molecular mechanisms of signaling by the gain-of-function EGFR mutations common in NSCLC. Our results in live cells support a model in which these mutations mediate signaling through enhanced dimerization in the absence of ligand via coordinated interactions that include ectodomain dimerization arm engagement. The altered ectodomain behavior induced by kinase domain mutations provides evidence for inside-out structural modulation, previously termed "inside-out signaling" (Macdonald-Obermann and Pike, 2009; Lu *et al.*, 2012), as a mechanism underlying aberrant activity by NSCLC-associated kinase mutants of EGFR. Our findings have implications for future therapeutic strategies, since it is clear that the constitutively active receptors studied here still require dimerization for oncogenic signaling, including engagement of the dimerization arm. Combinations of dimer-disrupting agents, which target the ectodomain, and kinase-selective inhibitors may offer a critical therapeutic advantage.

MATERIALS AND METHODS

Cell lines and reagents

CHO cells and HeLa were cultured in Dulbecco's Modified Eagle Medium (Life Technologies # 10313-021) supplemented with 10% fetal bovine serum (HyClone), penicillin-streptomycin, and 2 mM L-glutamine. Antibodies against phosphorylated EGFR (clone 1H12 #2236S) and total EGFR (clone 15F8, #4405S) used for immunoblotting and immunofluorescence were from Cell Signaling Technology. HRP conjugated goat anti-rabbit and anti-mouse secondary antibodies (sc-2004, sc-2005), and EGFR antibody used for super-resolution imaging (anti-EGFR, R-1, sc-101) were from Santa Cruz Biotechnology. Anti-HA-biotin (12158167001) and anti-HA-FITC (11988506001), high Affinity rat monoclonal antibody Fab fragments (clone 3F10) were purchased from Roche. EGF-biotin conjugate (E-3477), Qdot 585 streptavidin conjugate (Q10111MP), Qdot 655 streptavidin conjugate (Q10121MP), and Alexa Fluor 647 carboxylic acid, succinimidyl ester (A-20006) were purchased from Life Technologies. Cy3B NHS-ester (PA63100) was purchased from GE Healthcare Life Sciences.

Cloning and generation of stable cell lines

Cloning of HA-tagged and ACP-tagged EGFR constructs and mutations was performed as previously described (Ziomkiewicz *et al.*, 2013; Steinkamp *et al.*, 2014), inserting the HA-tag immediately downstream of the receptor signal peptide.

CHO cells were transfected with cDNA encoding either HA-tagged EGFR or ACP-tagged EGFR (WT, L858R, or ΔL747-P753insS) by Amaxa nucleofection. Briefly, $3x10^6$ cells were transfected with 4 μg DNA using Amaxa Nucleofection Kit V optimized for CHO cells per manufacturer's instructions. Cells were selected using 1 mg/ml G418 and sorted using either EGF-AlexaFluor488 (LifeTechnologies #E13345) or EGF-AlexaFluor647 (LifeTechnologies #E35351). After sorting, cells were maintained in G418 and routinely sorted, yielding a heterogeneous non-clonal population. Membrane localization of the HA- or ACP-tagged receptors was confirmed by live labeling, and activity and ligand-sensitivity of HA-EGFR or ACP-EGFR was confirmed by immunofluorescence and immunoblotting.

Transient transfection of HeLa cells

Before transfection, HeLa cells were grown to ~75% confluence. For transfection, $1.5x10^6$ cells were transfected with 2.5 μg of the indicated plasmid (pcDNA3.1+ HA-EGFR-WT, HA-EGFR-L858R, or HA-EGFR-L858R+246-253*) using Amaxa Nucleofection Kit R (Lonza) following manufacturer's instructions. Cells were immediately transferred to complete culture media and seeded onto 8-well chamber slides (Lab-Tec, Thermo Scientific #155411) for single particle tracking or immunofluorescence labeling. The remaining cells were plated onto a 100 mm dish for lysis and western blot analysis. Cells were incubated for ~24 hours at 37°C before single particle tracking (see below), fixation and immunolabeling, or lysis and western blot analysis. Separate transfections were done for independent experiments.

Immunoblotting

CHO cells expressing HA-EGFR (wild type or mutants) were seeded on 60 mm or 100 mm dishes and grown to ~80% confluency. Cells were pre-treated with tyrosine kinase inhibitor

as indicated followed by treatment with EGF (50 nM) for 8 minutes. After washing with cold PBS, cells were lysed in RIPA buffer on ice for 1 hour. Protein concentration of cleared lysates was measured by BCA assay (Pierce, Rockford IL), and equal amounts of total protein were separated on a 4-15% polyacrylamide gel (BioRad), transferred to nitrocellulose (iBlot transfer system, Life Technologies), probed with the indicated antibody, and imaged using enhanced chemiluminescence on a BioRad ChemiDoc.

Immunofluorescence

CHO cells expressing HA-EGFR (wild type or mutants) were seeded on 18 mm coverslips overnight and labeled live using an anti-HA-FITC (Fab) at 2 μg/ml for 1 hour at 37 °C in serum free media followed by four washes in serum free media. Cells were treated without or with dark (i.e. non-fluorescently labeled or unconjugated) EGF (50 nM) for 5 minutes and immediately fixed in 4% paraformaldehyde for 15 minutes. Cells were washed extensively with 10 mM Tris (pH 7.2) and PBS, and permeabilized with 0.1% Triton X-100 (w/v) in 5% BSA for 20 min. Cells were labeled with anti-pY1068 and an anti-mouse Alexa647 secondary antibody. Cells were mounted on slides using Prolong Gold with DAPI and imaged using a Zeiss LSM510. Immunofluorescence labeling of transiently transfected HeLa cells was carried out in 8-well chamber slides (Lab-Tec, Thermo Scientific #155411). All image processing was performed using Matlab (The MathWorks, Inc., Natick, MA) in conjunction with the image processing library DIPImage (Delft University of Technology).

Immunofluorescence assays of EGFR abundance and phosphorylation

For each confocal fluorescence image, total receptor abundance was characterized in terms of the per-pixel intensity of the receptor label (anti-HA FITC), and the level of receptor phosphorylation was similarly characterized using a site-specific antibody (α-pY1068 EGFR). After thresholding on total receptor intensity to mask the membrane of expressing cells, the total receptor intensity and corresponding phosphorylated EGFR level was averaged for each pixel to generate a plot showing the relationship between receptor expression and receptor phosphorylation (Figure 1C).

Model-based analysis of immunofluorescence data

See Supplementary Note.

Single particle tracking, image registration, and processing

Single- and dual-color SPT of unliganded and ligand-bound EGFR, diffusion analysis, and HMM analysis, were carried out using anti-HA- and EGF-conjugated QDs as previously described (Low-Nam *et al.*, 2011; Steinkamp *et al.*, 2014). Briefly, equal molar ratios of anti-HA-biotin or EGF-biotin and QD585 or QD655 streptavidin were incubated in PBS + 1% BSA at 4 °C for 2 hours with agitation before imaging. CHO cells expressing EGFR-WT, EGFR-L858R, or EGFR-ΔL747-P753insS were seeded in 8-well chamber slides (Lab-Tec, Thermo Scientific #155411) and allowed to adhere to the glass overnight. Cell culture media was exchanged for Tyrodes imaging buffer (135 mM NaCl, 10 mM KCl, 0.4 mM $MgCl_2$, 1 mM $CaCl_2$, 10 mM HEPES, 20 mM glucose, 0.1% BSA, pH 7.2), and cells were incubated with anti-HA-QD585/655 or EGF-QD585/655 to obtain single molecule density on the apical cell surface. After extensive washing with imaging buffer, cells were imaged for up to 8 minutes to avoid imaging of internalized receptors.

Wide field imaging for SPT was performed using an Olympus IX71 inverted microscope equipped with a 60× 1.2 N.A. water objective; an objective heater (Bioptechs, Butler, PA) maintained physiological temperature at 34-36 °C. Wide field excitation was provided by a mercury lamp with a 436/10 nm bandpass excitation filter and a 50/50 neutral density filter. Emission was collected by an EMCCD camera (Andor iXon 887) and pixel size was 166.67 nm. QD emission was collected using the OptoSplit image splitter (Cairn Research) to simultaneously image two spectrally distinct QDs, using a 600 nm dichroic and the appropriate filters, 655/40 nm and 585/20 nm bandpass filters (Chroma, Rockingham, VT). Fiducial channel registration datasets were acquired periodically using 0.2 μm Tetraspeck fluorescent beads (Invitrogen).

Single molecule localization and trajectory connection were carried out using GPU computing as previously described (Smith *et al.*, 2010). For details of SPT analysis, see Low-

Nam et al. (Low-Nam *et al.*, 2011). Diffusion analysis of trajectories was conducted by square displacement analysis and two-component fitting, as previously described (de Keijzer *et al.*, 2008; Low-Nam *et al.*, 2011). All image processing was performed using Matlab (The MathWorks, Inc., Natick, MA) in conjunction with the image processing library DIPImage (Delft University of Technology). Dimer events were identified using a three-state hidden Markov model (HMM), as previously described (Low-Nam *et al.*, 2011; Steinkamp *et al.*, 2014). The Viterbi algorithm (Forney, 1973) is used to identify the most likely state within individual QD interactions.

Super-resolution imaging and analysis

CHO cells expressing EGFR and mutants were washed with PBS and fixed in 4% paraformaldehyde + 0.2% glutaraldehyde for ~2 hours to minimize receptor mobility after fixation (Tanaka *et al.*, 2010). Cells were washed extensively with PBS, once with 0.1% $NaBH_4$, and once with 10 mM Tris-HCl (pH 7.2) to reduce background fluorescence and quench cross-linkers. After blocking with PBS + 2% BSA, cells were labeled with Alexa647- or Cy3B -conjugated monoclonal, primary antibodies against EGFR. Identical, monoclonal antibody against EGFR (anti-EGFR, R-1, Santa Cruz Biotechnology # sc-101) was used for Alexa647- and Cy3B-labeling. Alexa647-conjugated anti-EGFR was purchased commercially (Santa Cruz Biotechnology #sc-101 AF647), and Cy3B-conjugated antibody was made using the carrier-free version of anti-EGFR R-1 along with reactive Cy3B NHS-ester (GE Healthcare Life Sciences # PA63100). Cells were labeled with Alexa647- and Cy3B-conjugated anti-EGFR in a 1:1 ratio in PBS + 2% BSA either overnight at 4 °C or 2 hours at room temperature followed by extensive washing with PBS + 2% BSA. For activation of EGFR-WT, cells were exposed to 50 nM EGF for 8 minutes at room temperature prior to fixation; a sufficient concentration and duration to ensure dimerization of EGFR on the basal surface of the cell.

Two-color super-resolution imaging via direct stochastic optical reconstruction microscopy (dSTORM) was performed as described (van de Linde *et al.*, 2011) and analyzed similar to previously used techniques (Semrau *et al.*, 2011; Veatch *et al.*, 2012). Imaging was performed using an inverted microscope (IX71; Olympus America, Center Valley, PA) equipped with an oil-immersion objective 1.45-NA total internal reflection fluorescence objective (U-APO

150×/NA 1.45; Olympus America). A 637-nm laser (collimated from a laser diode, HL63133DG, Thorlabs) was used for Alexa647 excitation (~0.5 kW/cm^2), and a 561-nm laser (Sapphire 561, Coherrent, Inc.) was used for Cy3B excitation (~0.5 kW/cm^2). Additional 405 excitation (up to ~25 W/cm^2) was used for activation of both Alexa647 and Cy3B dyes as necessary. All laser light was configured in total internal reflection geometry. Cells were imaged in standard dSTORM imaging buffer (Dempsey *et al.*, 2011) with enzymatic oxygen scavenging system and primary thiol: 50mM Tris, 10mM NaCl, 10% w/v glucose, 168.8 U/ml glucose oxidase (Sigma #G2133) and 1404 U/ml catalase (Sigma #C9332), 10 mM 2-aminoethanethiol (MEA), pH 8.5.

A quad-band dichroic and emission filter set (LF405/488/561/635-A; Semrock, Rochester, NY) set was used for sample illumination and emission. Emission light was separated into two channels using a custom built emission filter setup using a 655 dichroic and the appropriate filters for Alexa647 (692/40 nm) and Cy3B (600/37 nm), directing emission light for Alexa647 and Cy3B onto different halves of an iXon 897 electron-multiplying charge-coupled device (EM CCD) camera (Andor Technologies, South Windsor, CT). The EMCCD gain was set to 200, and frames were 256 × 256 pixels (for each channel) with a pixel size of 106.7 nm. Images were acquired at maximum camera speed (~15 ms exposure for 256 × 256 pixel region) and a total of 10,000-20,000 frames were collected. The sample chamber was mounted in a three-dimensional piezostage (Nano-LPS; Mad City Labs, Madison, WI) with a resolution along the *xyz*-axes of 0.2 nm. Sample drift was corrected for throughout the imaging procedure using a custom-built stage stabilization routine.

Imaging was carried out sequentially starting with Alexa647 followed by Cy3B, and two-color super-resolution data was overlayed using an affine transformation matrix generated from the localization of fiducial beads with fluorescence emission in both channels from 0.2 μm Tetraspeck fluorescent beads (Invitrogen). Fiducial bead datasets were acquired periodically throughout imaging, and the overlay accuracy was calculated by applying the affine transformation matrix from one channel registration to other channel registration sets within a single day (Figure S9). The overlay error is given as a mean ± standard deviation of the root mean squared error.

Two-color super-resolution datasets were analyzed by localization-based cross-correlation analysis similar to previously described methods (Semrau *et al.*, 2011; Sengupta *et al.*, 2011; Veatch *et al.*, 2012; Shelby *et al.*, 2013). Briefly, a subregion within each cell (typically 25-100 μm^2, excluding the lateral membrane region) was selected, and opposite color localizations were binned radially in 20 nm bins. Data was normalized to total center counts and to the average number of localizations per unit area. Shown is the normalized radial distribution function (RDF) with 20 nm bin size of 10-20 cells imaged over several days, treating the RDF of each cell as independent (mean ± standard error).

Measurement and analysis of FLIM data

FRET measurements between EGFR and the plasma membrane were performed as previously described (Ziomkiewicz *et al.*, 2013).

Donor and acceptor cell labeling, spectra and R_0. The ACP-tagged EGFR expressing CHO cells were plated and grown in 4-well Lab-Tek chambered coverglass slides (Thermo Fisher) in DMEM with 10% FCS. Prior to imaging, cells were starved for 1 hour before labeling with 4 µM Oregon Green CoA in Tyrodes buffer containing 0.5% BSA and 10 mM $MgCl_2$ for 20 min at room temperature by addition of Sfp PPTase from *Bacillus subtilis* and washed 3 times over 15 minutes with RAB buffer before measuring. Acceptor NR12S (Kucherak *et al.*, 2010) (the kind gift of A. Klymchenko) was diluted from a DMSO stock with vigorous vortexing to 4 µM in Tyrodes buffer and immediately added to an equal volume of buffer on the cells with rapid mixing. The excitation and emission spectra of the donor and acceptor are shown in Figure S5. An R_0 of 5.8 nm was calculated from the Förster overlap integral. Figure S6 shows possible distances between the ACP tag and the cell membrane if the EGFR is in the inhibited, unliganded or the extended, liganded conformations.

*TCSPC Hardware***.** The excitation light source was a Fianium SC400-4-2 white-light laser system pulsed at 20 MHz that was coupled to an AOTFnC-400.650-TN, AA Optic set at 467 nm in the case of one system and the excitation wavelength isolated from a Fianium Whitelase SC450 by a 467/10 nm Semrock filter in the case of the other system. Excitation was directed into an IX71 Olympus microscope equipped with a 60x or 100x Olympus objective, 1.49 NA and a stage scanning system. Data acquisition was recorded with a 510/10nm Semrock

BP emission filter in front of a Micron Photon Devices (Bolzano, Italy) PDM Series SPAD detector coupled to a PicoQuant PicoHarp 300 TCSPC correlator. The data were collected at 32 ps/ch with 5 ms/pixel dwell time and a 0.5 μm/pixel resolution.

TCSPC Analysis Software. Multicomponent lifetime analysis routines were written in Mathematica (Wolfram Research). The IRF was fit to an analytical function (*pulse*) composed of a combination of a Gaussian and an integrated Gaussian·exponential functions. The entire course of the fluorescence response (*signal)* from cells exposed to excitation pulses were then fit to the analytical convolution of the IRF and 1,2, or 3 additional components according to the equations described in Ziomkiewicz et al. (Ziomkiewicz *et al.*, 2013). The fit parameters in *signal* are the lifetime (τ), and a corresponding amplitude, both of which can be determined for one or more components. Single pixel decays could only be fit by a single component. More precise two-component analyses were possible after ordering and binning of the pixel data into groups (generally 2-10, each with 10-1000 members) in order of decreasing peak signal magnitude. The first component was assigned to background and the second component assigned to the donor. In the case of unlabeled cells and cells labeled only with acceptor, fitting required only a corresponding amplitude factor. One- or two-sided masks were generated on the image data to restrict the analysis primarily to foreground pixels. Donor lifetimes were back-mapped onto the 2-D cell images. Derived amplitudes and lifetimes can be subjected to further analysis based on the corresponding images and two-dimensional histograms. Examples of the back-mapped data for ACP-EGFR-WT and ACP-EGFR-L858R are shown in Figure 4B and 4C (bottom row of images), respectively.

ACKNOWLEDGEMENTS

This study was supported by NSF MCB-0845062 (DSL), the Oxnard Foundation (DSL), NIH P50GM085273 (BSW) and NSF 0954836 (KAL). DJA-J received financial support from the Max-Planck Society. Financial support by the Deutsche Forschungsgemeinschaft is gratefully acknowledged (SFB 937, project A5). N.K. is grateful to the Niedersächsisches Ministerium für Wissenschaft and Kultur for a MWK stipend. Use of the UNM Cancer Center Microscopy and Flow Cytometry facilities, and NIH support for these cores, is acknowledged (http://hsc.unm.edu/crtc/microscopy/acknowledgement.shtml). We gratefully thank Thomas

Jovin for analysis of FRET/FLIM data, input regarding the equilibrium modeling (Supplementary Note), and insightful discussions. We thank Shalini T. Low-Nam, Samantha L. Schwartz, and Patrick J. Cutler for assistance with single particle tracking development and analysis. Additionally, we thank Jörg Enderlein for providing the TCSPC facilities for FLIM measurements, Andrey Klymchenko for the gift of the NR12S membrane probe, and Reinhard Klement for MD calculations.

REFERENCES

Abulrob, A., Lu, Z., Baumann, E., Vobornik, D., Taylor, R., Stanimirovic, D., and Johnston, L. J. (2010). Nanoscale imaging of epidermal growth factor receptor clustering: effects of inhibitors. J. Biol. Chem. *285*, 3145–3156.

Alvarado, D., Klein, D. E., and Lemmon, M. A. (2010). Structural basis for negative cooperativity in growth factor binding to an EGF receptor. Cell *142*, 568–579.

Arkhipov, A., Shan, Y., Das, R., Endres, N. F., Eastwood, M. P., Wemmer, D. E., Kuriyan, J., and Shaw, D. E. (2013). Architecture and Membrane Interactions of the EGF Receptor. Cell *152*, 557–569.

Bessman, N. J., and Lemmon, M. A. (2012). Finding the missing links in EGFR. Nat. Struct. Mol. Biol. *19*, 1–3.

Bos, M., Mendelsohn, J., Kim, Y. M., Albanell, J., Fry, D. W., and Baselga, J. (1997). PD153035, a tyrosine kinase inhibitor, prevents epidermal growth factor receptor activation and inhibits growth of cancer cells in a receptor number-dependent manner. Clin. Cancer Res. *3*, 2099–2106.

Bremer, E. G., Schlessinger, J., and Hakomori, S. (1986). Ganglioside-mediated modulation of cell growth. Specific effects of GM3 on tyrosine phosphorylation of the epidermal growth factor receptor. J. Biol. Chem. *261*, 2434–2440.

Burgess, A. W., Cho, H., Eigenbrot, C., Ferguson, K. M., Garrett, T. P. J., Leahy, D. J., Lemmon, M. A., Sliwkowski, M. X., Ward, C. W., and Yokoyama, S. (2003). An open-and-shut case? Recent insights into the activation of EGF/ErbB receptors. Mol. Cell *12*, 541–552.

Carey, K. D., Garton, A. J., Romero, M. S., Kahler, J., Thomson, S., Ross, S., Park, F., Haley, J. D., Gibson, N., and Sliwkowski, M. X. (2006). Kinetic analysis of epidermal growth factor receptor somatic mutant proteins shows increased sensitivity to the epidermal growth factor receptor tyrosine kinase inhibitor, erlotinib. Cancer Res. *66*, 8163–8171.

Carraway, K. L., Koland, J. G., and Cerione, R. A. (1989). Visualization of epidermal growth factor (EGF) receptor aggregation in plasma membranes by fluorescence resonance energy transfer. Correlation of receptor activation with aggregation. J. Biol. Chem. *264*, 8699–8707.

Cho, J. *et al.* (2013). Cetuximab response of lung cancer-derived EGF receptor mutants is associated with asymmetric dimerization. Cancer Res. *73*, 6770–6779.

Choi, S. H., Mendrola, J. M., and Lemmon, M. A. (2007). EGF-independent activation of cell-surface EGF receptors harboring mutations found in gefitinib-sensitive lung cancer. Oncogene *26*, 1567–1576.

Chung, I., Akita, R., Vandlen, R., Toomre, D., Schlessinger, J., and Mellman, I. (2010). Spatial control of EGF receptor activation by reversible dimerization on living cells. Nature *464*, 783–787.

Clayton, A. H. A., Walker, F., Orchard, S. G., Henderson, C., Fuchs, D., Rothacker, J., Nice, E. C., and Burgess, A. W. (2005). Ligand-induced dimer-tetramer transition during the activation of the cell surface epidermal growth factor receptor-A multidimensional microscopy analysis. J. Biol. Chem. *280*, 30392–30399.

Coskun, Ü., Grzybek, M., Drechsel, D., and Simons, K. (2011). Regulation of human EGF receptor by lipids. Proc. Natl. Acad. Sci. U. S. A. *108*, 9044–9048.

Dahan, M., Lévi, S., Luccardini, C., Rostaing, P., Riveau, B., and Triller, A. (2003). Diffusion dynamics of glycine receptors revealed by single-quantum dot tracking. Science *302*, 442–445.

Dawson, J. P., Berger, M. B., Lin, C., Schlessinger, J., Lemmon, M. A., and Ferguson, K. M. (2005). Epidermal growth factor receptor dimerization and activation require ligand-induced conformational changes in the dimer interface. Mol. Cell. Biol. *25*, 7734–7742.

Dempsey, G. T., Vaughan, J. C., Chen, K. H., Bates, M., and Zhuang, X. (2011). Evaluation of fluorophores for optimal performance in localization-based super-resolution imaging. Nat. Methods *8*, 1027–1036.

Endres, N. F. *et al.* (2013). Conformational Coupling across the Plasma Membrane in Activation of the EGF Receptor. Cell *152*, 543–556.

Forney, G. D. (1973). The Viterbi Algorithm. Proc. IEEE *61*, 268–278.

Gan, H. K., Kaye, A. H., and Luwor, R. B. (2009). The EGFRvIII variant in glioblastoma multiforme. J. Clin. Neurosci. *16*, 748–754.

Godin-Heymann, N., Ulkus, L., Brannigan, B. W., McDermott, U., Lamb, J., Maheswaran, S., Settleman, J., and Haber, D. A. (2008). The T790M “gatekeeper” mutation in EGFR mediates resistance to low concentrations of an irreversible EGFR inhibitor. Mol. Cancer Ther. *7*, 874–879.

Greulich, H. *et al.* (2005). Oncogenic transformation by inhibitor-sensitive and -resistant EGFR mutants. PLoS Med. *2*, e313.

Hanold, L. E., Oruganty, K., Ton, N. T., Beedle, A. M., Kannan, N., and Kennedy, E. J. (2015a). Inhibiting EGFR dimerization using triazolyl-bridged dimerization arm mimics. PLoS One *10*, e0118796.

Hanold, L. E., Watkins, C. P., Ton, N. T., Liaw, P., Beedle, A. M., and Kennedy, E. J. (2015b). Design of a selenylsulfide-bridged EGFR dimerization arm mimic. Bioorg. Med. Chem.

Heilemann, M., Linde, S., Schüttpelz, M., Kasper, R., Seefeldt, B., Mukherjee, A., Tinnefeld, P., and Sauer, M. (2008). Subdiffraction-resolution fluorescence imaging with conventional fluorescent probes. Angew. Chem. Int. Ed. Engl. *47*, 6172–6176.

Hendriks, B. S., Opresko, L. K., Wiley, H. S., and Lauffenburger, D. (2003). Coregulation of epidermal growth factor receptor/human epidermal growth factor receptor 2 (HER2) levels and locations: quantitative analysis of HER2 overexpression effects. Cancer Res. *63*, 1130–1137.

Jiang, J., Greulich, H., Jänne, P. a, Sellers, W. R., Meyerson, M., and Griffin, J. D. (2005). Epidermal growth factor-independent transformation of Ba/F3 cells with cancer-derived epidermal growth factor receptor mutants induces gefitinib-sensitive cell cycle progression. Cancer Res. *65*, 8968–8974.

Jura, N., Endres, N. F., Engel, K., Deindl, S., Das, R., Lamers, M. H., Wemmer, D. E., Zhang, X., and Kuriyan, J. (2009). Mechanism for activation of the EGF receptor catalytic domain by the juxtamembrane segment. Cell *137*, 1293–1307.

Kästner, J., Loeffler, H. H., Roberts, S. K., Martin-Fernandez, M. L., and Winn, M. D. (2009). Ectodomain orientation, conformational plasticity and oligomerization of ErbB1 receptors investigated by molecular dynamics. J. Struct. Biol. *167*, 117–128.

Kaszuba, K., Grzybek, M., Orłowski, A., Danne, R., Róg, T., Simons, K., Coskun, Ü., and Vattulainen, I. (2015). N-Glycosylation as determinant of epidermal growth factor receptor conformation in membranes. Proc. Natl. Acad. Sci. U. S. A. *112*.

Keating, E., Nohe, A., and Petersen, N. O. (2008). Studies of distribution, location and dynamic properties of EGFR on the cell surface measured by image correlation spectroscopy. Eur. Biophys. J. *37*, 469–481.

De Keijzer, S., Sergé, A., van Hemert, F., Lommerse, P. H. M., Lamers, G. E. M., Spaink, H. P., Schmidt, T., and Snaar-Jagalska, B. E. (2008). A spatially restricted increase in receptor mobility is involved in directional sensing during Dictyostelium discoideum chemotaxis. J. Cell Sci. *121*, 1750–1757.

Kobayashi, S., Boggon, T. J., Dayaram, T., Jänne, P. A., Kocher, O., Meyerson, M., Johnson, B. E., Eck, M. J., Tenen, D. G., and Halmos, B. (2005). EGFR mutation and resistance of non-small-cell lung cancer to gefitinib. N. Engl. J. Med. *352*, 786–792.

Kozer, N., Barua, D., Henderson, C., Nice, E. C., Burgess, A. W., Hlavacek, W. S., and Clayton, A. H. a (2014). Recruitment of the adaptor protein Grb2 to EGFR tetramers. Biochemistry *53*, 2594–2604.

Kozer, N., Barua, D., Orchard, S., Nice, E. C., Burgess, A. W., Hlavacek, W. S., and Clayton, A. H. A. (2013). Exploring higher-order EGFR oligomerisation and phosphorylation--a combined experimental and theoretical approach. Mol. Biosyst. *9*, 1849–1863.

Kozer, N., Henderson, C., Jackson, J. T., Nice, E. C., Burgess, A. W., and Clayton, A. H. A. (2011). Evidence for extended YFP-EGFR dimers in the absence of ligand on the surface of living cells. Phys. Biol. *8*, 066002.

Kucherak, O. A., Oncul, S., Darwich, Z., Yushchenko, D. A., Arntz, Y., Didier, P., Mély, Y., and Klymchenko, A. S. (2010). Switchable nile red-based probe for cholesterol and lipid order at the outer leaflet of biomembranes. J. Am. Chem. Soc. *132*, 4907–4916.

Lemmon, M. A., and Schlessinger, J. (2010). Cell signaling by receptor tyrosine kinases. Cell *141*, 1117–1134.

Li, S., Kussie, P., and Ferguson, K. M. (2008). Structural basis for EGF receptor inhibition by the therapeutic antibody IMC-11F8. Structure *16*, 216–227.

Li, S., Schmitz, K. R., Jeffrey, P. D., Wiltzius, J. J. W., Kussie, P., and Ferguson, K. M. (2005). Structural basis for inhibition of the epidermal growth factor receptor by cetuximab. Cancer Cell *7*, 301–311.

Lidke, D. S., Lidke, K. A., Rieger, B., Jovin, T. M., and Arndt-Jovin, D. J. (2005). Reaching out for signals: filopodia sense EGF and respond by directed retrograde transport of activated receptors. J. Cell Biol. *170*, 619–626.

Lidke, D. S., Nagy, P., Barisas, B. G., Heintzmann, R., Post, J. N., Lidke, K. A., Clayton, A. H. A., Arndt-Jovin, D. J., and Jovin, T. M. (2003). Imaging molecular interactions in cells by dynamic and static fluorescence anisotropy (rFLIM and emFRET). Biochem. Soc. Trans. *31*, 1020–1027.

Lidke, D. S., Nagy, P., Heintzmann, R., Arndt-Jovin, D. J., Post, J. N., Grecco, H. E., Jares-Erijman, E. a, and Jovin, T. M. (2004). Quantum dot ligands provide new insights into erbB/HER receptor-mediated signal transduction. Nat. Biotechnol. *22*, 198–203.

Van de Linde, S., Löschberger, A., Klein, T., Heidbreder, M., Wolter, S., Heilemann, M., and Sauer, M. (2011). Direct stochastic optical reconstruction microscopy with standard fluorescent probes. Nat. Protoc. *6*, 991–1009.

Low-Nam, S. T., Lidke, K. A., Cutler, P. J., Roovers, R. C., van Bergen en Henegouwen, P. M. P., Wilson, B. S., and Lidke, D. S. (2011). ErbB1 dimerization is promoted by domain co-confinement and stabilized by ligand binding. Nat. Struct. Mol. Biol. *18*, 1244–1249.

Lu, C., Mi, L.-Z., Grey, M. J., Zhu, J., Graef, E., Yokoyama, S., and Springer, T. a. (2010). Structural evidence for loose linkage between ligand binding and kinase activation in the epidermal growth factor receptor. Mol. Cell. Biol. *30*, 5432–5443.

Lu, C., Mi, L.-Z., Schürpf, T., Walz, T., and Springer, T. a. (2012). Mechanisms for kinase-mediated dimerization of the epidermal growth factor receptor. J. Biol. Chem. *287*, 38244–38253.

Lynch, T. J. *et al.* (2004). Activating mutations in the epidermal growth factor receptor underlying responsiveness of non-small-cell lung cancer to gefitinib. N. Engl. J. Med. *350*, 2129–2139.

Macdonald, J. L., and Pike, L. J. (2008). Heterogeneity in EGF-binding affinities arises from negative cooperativity in an aggregating system. Proc. Natl. Acad. Sci. U. S. A. *105*, 112–117.

Macdonald-Obermann, J. L., and Pike, L. J. (2009). The intracellular juxtamembrane domain of the epidermal growth factor (EGF) receptor is responsible for the allosteric regulation of EGF binding. J. Biol. Chem. *284*, 13570–13576.

Martin-Fernandez, M. L., Clarke, D. T., Tobin, M. J., Jones, S. V, and Jones, G. R. (2002). Preformed oligomeric epidermal growth factor receptors undergo an ectodomain structure change during signaling. Biophys. J. *82*, 2415–2427.

Mattoon, D., Klein, P., Lemmon, M. A., Lax, I., and Schlessinger, J. (2004). The tethered configuration of the EGF receptor extracellular domain exerts only a limited control of receptor function. Proc. Natl. Acad. Sci. U. S. A. *101*, 923–928.

McLaughlin, S., Smith, S. O., Hayman, M. J., and Murray, D. (2005). An electrostatic engine model for autoinhibition and activation of the epidermal growth factor receptor (EGFR/ErbB) family. J. Gen. Physiol. *126*, 41–53.

Mi, L.-Z., Grey, M. J., Nishida, N., Walz, T., Lu, C., and Springer, T. a. (2008). Functional and Structural Stability of the Epidermal Growth Factor Receptor in Detergent Micelles and Phospholipid Nanodiscs †. Biochemistry *47*, 10314–10323.

Mi, L.-Z., Lu, C., Li, Z., Nishida, N., Walz, T., and Springer, T. a. (2011). Simultaneous visualization of the extracellular and cytoplasmic domains of the epidermal growth factor receptor. Nat. Struct. Mol. Biol. *18*, 984–989.

Nagy, P., Claus, J., Jovin, T. M., and Arndt-Jovin, D. J. (2010). Distribution of resting and ligand-bound ErbB1 and ErbB2 receptor tyrosine kinases in living cells using number and brightness analysis. Proc. Natl. Acad. Sci. U. S. A. *107*, 16524–16529.

Needham, S. R., Hirsch, M., Rolfe, D. J., Clarke, D. T., Zanetti-Domingues, L. C., Wareham, R., and Martin-Fernandez, M. L. (2013). Measuring EGFR Separations on Cells with ~10 nm Resolution via Fluorophore Localization Imaging with Photobleaching. PLoS One *8*, e62331.

Needham, S. R., Zanetti-Domingues, L. C., Hirsch, M., Rolfe, D. J., Tynan, C. J., Roberts, S. K., Martin-Fernandez, M. L., and Clarke, D. T. (2014). Structure-function relationships and supramolecular organization of the EGFR (epidermal growth factor receptor) on the cell surface. Biochem. Soc. Trans. *42*, 114–119.

Ogiso, H. *et al.* (2002). Crystal structure of the complex of human epidermal growth factor and receptor extracellular domains. Cell *110*, 775–787.

Paez, J. G. *et al.* (2004). EGFR mutations in lung cancer: correlation with clinical response to gefitinib therapy. Science *304*, 1497–1500.

Pao, W. *et al.* (2004). EGF receptor gene mutations are common in lung cancers from "never smokers" and are associated with sensitivity of tumors to gefitinib and erlotinib. Proc. Natl. Acad. Sci. U. S. A. *101*, 13306–13311.

Pao, W., and Chmielecki, J. (2010). Rational, biologically based treatment of EGFR-mutant non-small-cell lung cancer. Nat. Rev. Cancer *10*, 760–774.

Pao, W., Miller, V. a, Politi, K. a, Riely, G. J., Somwar, R., Zakowski, M. F., Kris, M. G., and Varmus, H. (2005). Acquired resistance of lung adenocarcinomas to gefitinib or erlotinib is associated with a second mutation in the EGFR kinase domain. PLoS Med. *2*, e73.

Red-Brewer, M. L., Choi, S. H., Alvarado, D., Moravcevic, K., Pozzi, A., Lemmon, M. A., and Carpenter, G. (2009). The juxtamembrane region of the EGF receptor functions as an activation domain. Mol. Cell *34*, 641–651.

Red-Brewer, M. L., Yun, C.-H., Lai, D., Lemmon, M. A., Eck, M. J., and Pao, W. (2013). Mechanism for activation of mutated epidermal growth factor receptors in lung cancer. Proc. Natl. Acad. Sci. U. S. A.

Rivera, F., Vega-Villegas, M. E., Lopez-Brea, M. F., and Marquez, R. (2008). Current situation of Panitumumab, Matuzumab, Nimotuzumab and Zalutumumab. Acta Oncol. *47*, 9–19.

Sako, Y., Minoghchi, S., and Yanagida, T. (2000). Single-molecule imaging of EGFR signalling on the surface of living cells. Nat. Cell Biol. *2*, 168–172.

Schlessinger, J. (2002). Ligand-induced, receptor-mediated dimerization and activation of EGF receptor. Cell *110*, 669–672.

Schmiedel, J., Blaukat, A., Li, S., Knöchel, T., and Ferguson, K. M. (2008). Matuzumab binding to EGFR prevents the conformational rearrangement required for dimerization. Cancer Cell *13*, 365–373.

Schwartz, S. L., Yan, Q., Telmer, C. A., Lidke, K. A., Bruchez, M. P., and Lidke, D. S. (2015). Fluorogen-activating proteins provide tunable labeling densities for tracking FcεRI independent of IgE. ACS Chem. Biol. *10*, 539–546.

Semrau, S., Holtzer, L., González-Gaitán, M., and Schmidt, T. (2011). Quantification of Biological Interactions with Particle Image Cross-Correlation Spectroscopy (PICCS). Biophys. J. *100*, 1810–1818.

Sengupta, P., Jovanovic-Talisman, T., Skoko, D., Renz, M., Veatch, S. L., and Lippincott-Schwartz, J. (2011). Probing protein heterogeneity in the plasma membrane using PALM and pair correlation analysis. Nat. Methods *8*, 969–975.

Shan, Y., Eastwood, M. P., Zhang, X., Kim, E. T., Arkhipov, A., Dror, R. O., Jumper, J., Kuriyan, J., and Shaw, D. E. (2012). Oncogenic mutations counteract intrinsic disorder in the EGFR kinase and promote receptor dimerization. Cell *149*, 860–870.

Sharma, S. V, Bell, D. W., Settleman, J., and Haber, D. a (2007). Epidermal growth factor receptor mutations in lung cancer. Nat. Rev. Cancer *7*, 169–181.

Shelby, S. A., Holowka, D., Baird, B., and Veatch, S. L. (2013). Distinct stages of stimulated FcεRI receptor clustering and immobilization are identified through superresolution imaging. Biophys. J. *105*, 2343–2354.

Smith, C. S., Joseph, N., Rieger, B., and Lidke, K. A. (2010). Fast, single-molecule localization that achieves theoretically minimum uncertainty. Nat. Methods *7*, 373–375.

Steinkamp, M. P., Low-Nam, S. T., Yang, S., Lidke, K. a, Lidke, D. S., and Wilson, B. S. (2014). erbB3 is an active tyrosine kinase capable of homo- and heterointeractions. Mol. Cell. Biol. *34*, 965–977.

Talavera, A. *et al.* (2009). Nimotuzumab, an antitumor antibody that targets the epidermal growth factor receptor, blocks ligand binding while permitting the active receptor conformation. Cancer Res. *69*, 5851–5859.

Tanaka, K. A. K. *et al.* (2010). Membrane molecules mobile even after chemical fixation. Nat. Methods *7*, 865–866.

Thiel, K. W., and Carpenter, G. (2007). Epidermal growth factor receptor juxtamembrane region regulates allosteric tyrosine kinase activation. Proc. Natl. Acad. Sci. U. S. A. *104*, 19238–19243.

Tynan, C. J., Roberts, S. K., Rolfe, D. J., Clarke, D. T., Loeffler, H. H., Kästner, J., Winn, M. D., Parker, P. J., and Martin-Fernandez, M. L. (2011). Human epidermal growth factor receptor (EGFR) aligned on the plasma membrane adopts key features of Drosophila EGFR asymmetry. Mol. Cell. Biol. *31*, 2241–2252.

Valley, C. C., Lidke, K. A., and Lidke, D. S. (2014). The spatiotemporal organization of ErbB receptors: insights from microscopy. Cold Spring Harb. Perspect. Biol. *6*.

Veatch, S. L., Machta, B. B., Shelby, S. A., Chiang, E. N., Holowka, D. A., and Baird, B. A. (2012). Correlation functions quantify super-resolution images and estimate apparent clustering due to over-counting. PLoS One *7*, e31457.

Wang, Z., Longo, P. a, Tarrant, M. K., Kim, K., Head, S., Leahy, D. J., and Cole, P. a (2011). Mechanistic insights into the activation of oncogenic forms of EGF receptor. Nat. Struct. Mol. Biol. *18*, 1388–1393.

Webb, S. E. D., Roberts, S. K., Needham, S. R., Tynan, C. J., Rolfe, D. J., Winn, M. D., Clarke, D. T., Barraclough, R., and Martin-Fernandez, M. L. (2008). Single-molecule imaging and fluorescence lifetime imaging microscopy show different structures for high- and low-affinity epidermal growth factor receptors in A431 cells. Biophys. J. *94*, 803–819.

Yun, C.-H., Boggon, T. J., Li, Y., Woo, M. S., Greulich, H., Meyerson, M., and Eck, M. J. (2007). Structures of lung cancer-derived EGFR mutants and inhibitor complexes: mechanism of activation and insights into differential inhibitor sensitivity. Cancer Cell *11*, 217–227.

Yun, C.-H., Mengwasser, K. E., Toms, A. V, Woo, M. S., Greulich, H., Wong, K.-K., Meyerson, M., and Eck, M. J. (2008). The T790M mutation in EGFR kinase causes drug resistance by increasing the affinity for ATP. Proc. Natl. Acad. Sci. U. S. A. *105*, 2070–2075.

Zhang, X., Gureasko, J., Shen, K., Cole, P. A., and Kuriyan, J. (2006). An allosteric mechanism for activation of the kinase domain of epidermal growth factor receptor. Cell *125*, 1137–1149.

Ziomkiewicz, I., Loman, A., Klement, R., Fritsch, C., Klymchenko, A. S., Bunt, G., Jovin, T. M., and Arndt-Jovin, D. J. (2013). Dynamic conformational transitions of the EGF receptor in living mammalian cells determined by FRET and fluorescence lifetime imaging microscopy. Cytometry. A *83*, 794–805.

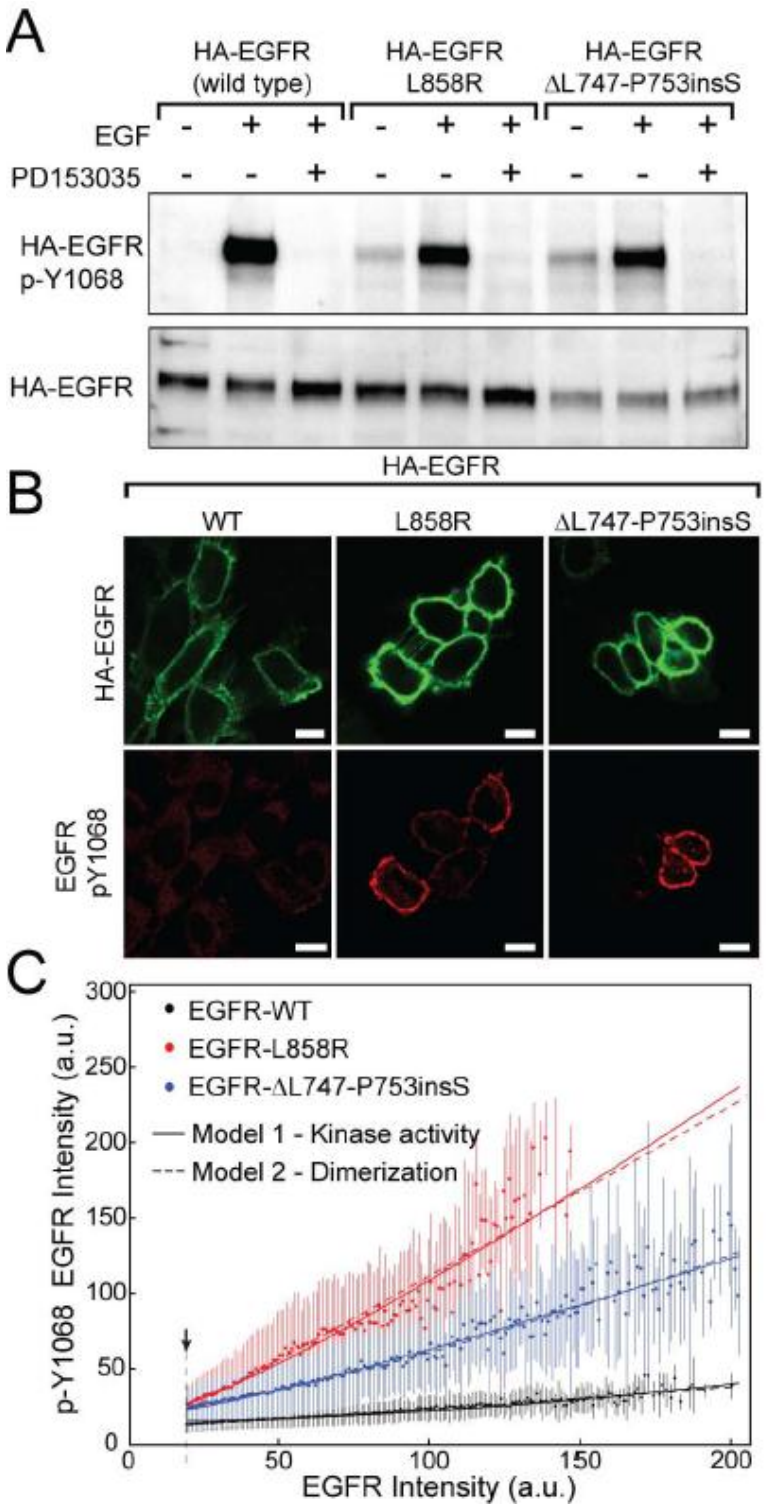
A
HA-EGFR (wild type)
HA-EGFR L858R
HA-EGFR ΔL747-P753insS
EGF
PD153035
HA-EGFR p-Y1068
HA-EGFR
B
HA-EGFR
WT
L858R
ΔL747-P753insS
HA-EGFR
EGFR pY1068
C
EGFR-WT
EGFR-L858R
EGFR-ΔL747-P753insS
Model 1 - Kinase activity
Model 2 - Dimerization
p-Y1068 EGFR Intensity (a.u.)
EGFR Intensity (a.u.)
0
50
100
150
200
250
300

Figure 1. Non-small cell lung carcinoma-associated EGFR kinase domain mutants are constitutively active and show increased phosphorylation with increasing receptor expression. (A) CHO cells expressing HA-tagged EGFR (HA-EGFR): EGFR-WT, EGFR-L858R, or EGFR-ΔL747-P753insS were serum starved followed by treatment without and with EGF. Cells were pre-treated with tyrosine kinase inhibitor PD153035 (1 μM) as indicated. Lysates were probed for phosphorylated EGFR (top) as well as total EGFR (bottom). **(B)** CHO cells expressing the indicated EGFR construct were labeled with a FITC-labeled α-HA Fab (green), then fixed, permeabilized, and labeled using α-pY1068 (red). **(C)** Cells imaged as in **(B)** were quantified for EGFR expression and phosphorylation. Each data point represents the mean pY1068 fluorescence intensity for a given EGFR intensity value per pixel across multiple images after thresholding (arrowhead and dashed line) to eliminate contribution from cells with no detectable EGFR expression; error bars illustrate the standard deviation of the measurement. Solid curves were obtained from Model 1 (Eqs. (5) and (6) with the constraints on parameter values indicated in Supplemental Methods); these curves reflect differences in the kinase activities of mutant and wild type forms of EGFR. Dashed curves were obtained from Model 2 (Eqs. (5) and (6) with the constraints on parameter values indicated in Supplemental Methods); these curves reflect differences in dimerization affinities of mutant and wild type forms of EGFR. Best-fit values for Model 1 and Model 2 and confidence limits from bootstrapping are given in Table S3. Individual plots for EGFR-WT, -L858R, and - ΔL747-P753insS are shown in Figure S2. A complete description each model is provided in Supplementary Note.

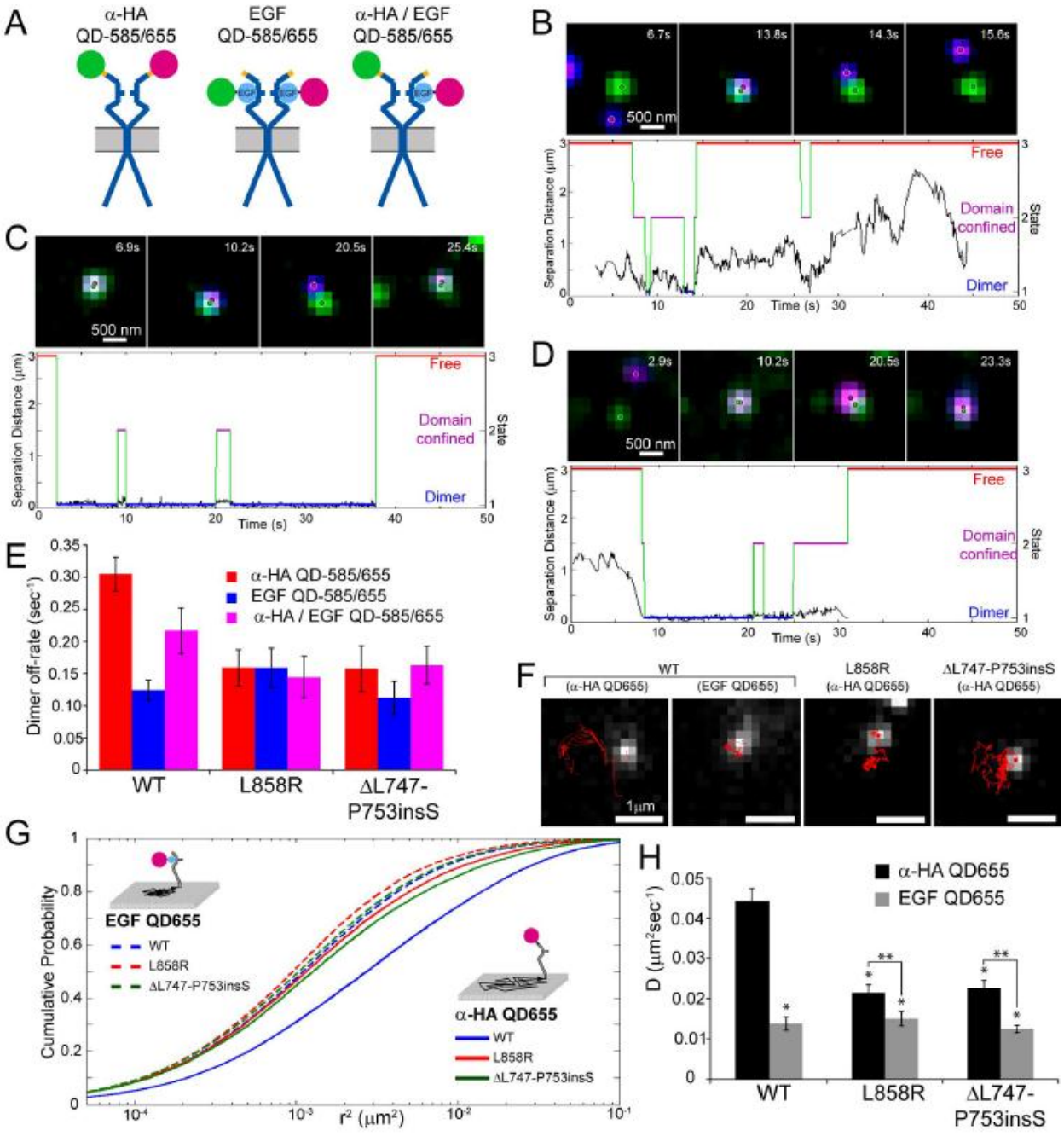
A
α-HA QD-585/655
EGF QD-585/655
α-HA / EGF QD-585/655
B
6.7s
13.8s
14.3s
15.6s
500 nm
Separation Distance (μm)
Free
Domain confined
Dimer
State
Time (s)
C
6.9s
10.2s
20.5s
25.4s
500 nm
D
2.9s
10.2s
20.5s
23.3s
500 nm
E
Dimer off-rate (sec⁻¹)
α-HA QD-585/655
EGF QD-585/655
α-HA / EGF QD-585/655
WT
L858R
ΔL747-P753insS
F
WT
(α-HA QD655)
(EGF QD655)
L858R
(α-HA QD655)
ΔL747-P753insS
(α-HA QD655)
1μm
G
Cumulative Probability
EGF QD655
WT
L858R
ΔL747-P753insS
α-HA QD655
WT
L858R
ΔL747-P753insS
r² (μm²)
H
D (μm²sec⁻¹)
α-HA QD655
EGF QD655
WT
L858R
ΔL747-P753insS

Figure 2. Detection of dimerization events by EGFR-WT and mutants on the surface of living cells using two-color SPT. (A) Schematic of EGFR dimers species identified using two-color QD tracking, including unliganded receptor dimers (0-EGF:2-EGFR, left), EGF-bound receptor dimers (2-EGF:2-EGFR, center), and singly-liganded EGFR dimers (1-EGF:2-EGFR, right). **(B-D)** Top: Raw, diffraction-limited data (pixelated, Gaussian-filtered green/magenta image) and corresponding localizations (green/magenta circles) for two-color SPT of EGFR dimerization. Bottom: Plot showing the changes in separation distance for the corresponding pair over time, overlaid with the resulting state assignments from the Viterbi analysis (Free, Domain Confined, or Dimer). Shown are EGFR-WT in the absence of ligand, tracking with QD-HA **(B)**, EGFR-WT bound to EGF, tracking with EGF-QD **(C)**, and EGFR-L858R in the absence of ligand, tracking with QD-HA **(D)**. Note the difference in dimer duration between conditions. **(E)** The dimer off-rates calculated from the HMM analysis confirm that mutants form stable dimers in the absence of ligand. **(F)** Raw data (pixelated images) and corresponding trajectories (red lines) for unliganded EGFR-WT, ligand-bound EGFR-WT, unliganded EGFR-L858R, and unliganded EGFR-ΔL747-P753insS illustrating differences in receptor mobility. The trajectory in each figure represents 20 seconds of tracked data. Scale bar is 1μm. **(G)** Receptor mobility was quantified using a cumulative probability plot of squared displacements. Solid lines represent unliganded EGFR tracked with QD-HA, and dashed lines represent ligand-bound receptor tracked with EGF-QD (see schematic inset). Shown are EGFR-WT (blue), EGFR-L858R (red) and EGFR-ΔL747-P753insS (green). **(H)** Diffusion coefficients determined from fitting the distribution of squared displacements for EGFR and mutants, both unliganded (black bars) and ligand-bound (gray bars). Shown is the mean ± standard error for a minimum of three independent experiments (* $p < 0.001$ relative to the unliganded EGFR-WT, and ** $p < 0.05$ comparing unliganded and ligand-bound EGFR-L858R or EGFR-ΔL747-P753insS). Dimer off-rates and diffusion values are summarized in Table S1.

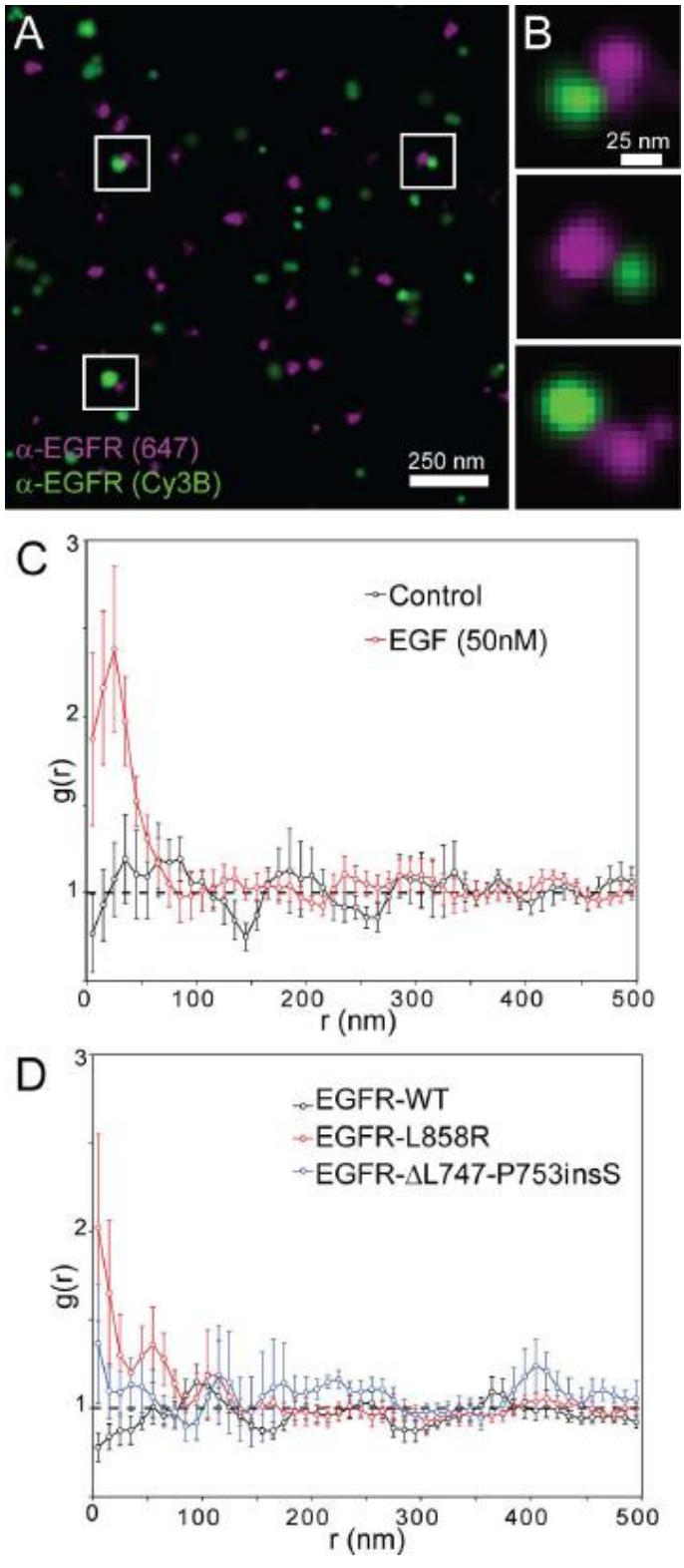
A
B
25 nm
α-EGFR (647)
α-EGFR (Cy3B)
250 nm
C
Control
EGF (50nM)
g(r)
r (nm)
D
EGFR-WT
EGFR-L858R
EGFR-ΔL747-P753insS
g(r)
r (nm)

Figure 3. Two-color dSTORM super-resolution imaging shows ligand induced EGFR dimerization and ligand-independent dimerization of EGFR mutants. (A) Representative two-color dSTORM reconstructed image of a CHO cell expressing EGFR-WT in the presence of EGF, fixed and labeled with a monoclonal anti-EGFR antibody conjugated with either Alexa647 (magenta) or Cy3B (green). Shown is a reconstructed superresolution image, where each localization is represented as a 2D Gaussian with σ proportional to its localization precision. The mean localization precision for Alexa647 and Cy3B is approximately 10 and 12 nm, respectively. **(B)** Zoomed regions of **(A)** highlighting potential EGFR dimers (white boxes) separated by < 50 nm. **(C)** Cross-correlation analysis of Alexa647 and Cy3B channels clearly shows EGFR-WT clustering after stimulation with EGF (red), indicated by the peak in the radial distribution function at short distances (< 50 nm) relative to control cells (black). The cross-correlation for control cells (black) remains flat, indicating no spatial correlation in the absence of ligand. **(D)** Similar two-color super-resolution and cross-correlation analysis in resting cells expressing EGFR mutants shows ligand-independent aggregation of EGFR-L858R (red) and EGFR-ΔL747-P753insS (blue), indicated by the increase in the radial distribution function at short distances (< 50 nm). EGFR-WT remains flat (black), indicating little aggregation in the absence of ligand.

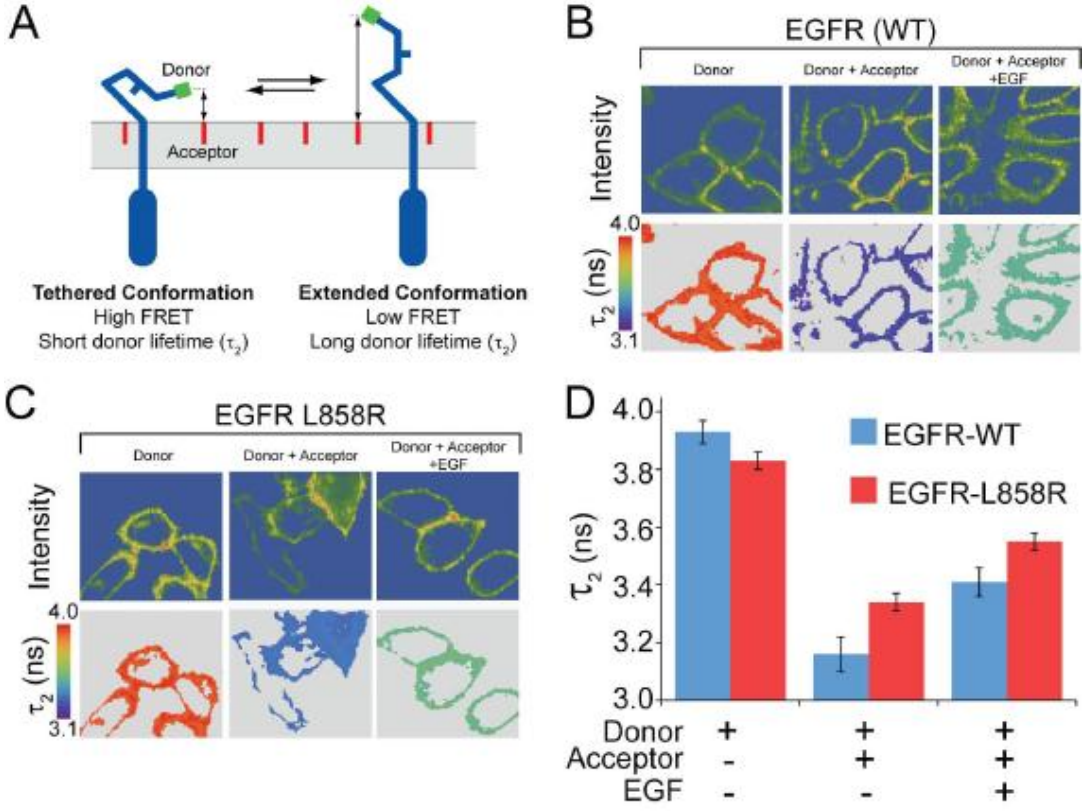
A
Donor
Acceptor
Tethered Conformation
High FRET
Short donor lifetime (τ_2)
Extended Conformation
Low FRET
Long donor lifetime (τ_2)
B
EGFR (WT)
Donor
Donor + Acceptor
Donor + Acceptor +EGF
Intensity
4.0
τ_2 (ns)
3.1
C
EGFR L858R
Donor
Donor + Acceptor
Donor + Acceptor +EGF
Intensity
4.0
τ_2 (ns)
3.1
D
4.0
3.8
3.6
3.4
3.2
3.0
τ_2 (ns)
EGFR-WT
EGFR-L858R
Donor + + +
Acceptor - + +
EGF - - +

Figure 4. FRET-FLIM and structural mutations reveal that unliganded EGFR-L858R adopts the extended conformation and requires ectodomain interactions for signaling. (A) Schematic of the EGFR ectodomain in the tethered, autoinhibited conformation (left) and the extended conformation (right). The donor fluorophore (Oregon Green 488, green) is covalently linked at the EGFR N-terminus via a small acyl carrier protein (ACP) tag, and the acceptor fluorophore (NR12S, a derivate of Nile Red, red) is embedded in the outer leaflet of the plasma membrane. By measuring FRET between donor and acceptor, the relative apparent separation between the EGFR N-terminus and the plasma membrane was determined. **(B-C)** Images of EGFR-WT **(B)** or EGFR-L858R **(C)** cells labeled with donor only (D only, left), donor with acceptor (D + A, middle), and donor with acceptor in the presence of EGF (D + A + EGF, right). Shown are the masked intensity images restricted primarily to the plasma membrane (top) and donor fluorescence lifetime values, τ_2, corresponding to the masked pixels (bottom). **(D)** Donor fluorescence lifetime values were averaged over many cells from 5-6 independent experiments for EGFR-WT and EGFR-L858R ± 2 μM NR12S acceptor and ± 30 nM EGF. Fluorescence lifetime results are summarized in Table S2.

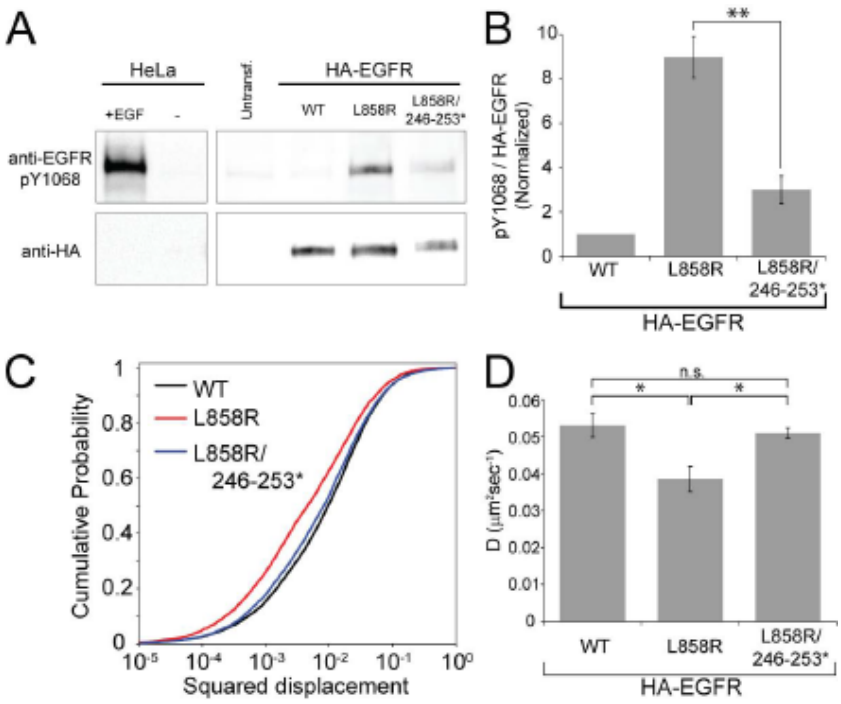

Figure 5. Ectodomain engagement is required for robust ligand-independent activity of EGFR-L858R. (A-B) Mutation of the EGFR dimerization arm within the context of the L858R kinase mutant causes a decrease in receptor phosphorylation at Y1068. HeLa cells were transfected with HA-EGFR-WT, -L858R, or -L858R/246-253* followed by lysis and analysis via western blot **(A)** and quantification **(B)**. Shown is the mean ± s.e.m of four independent experiments (* $p < 0.01$). **(C-D)** Single color QD tracking of HA-EGFR-WT, -L858R, and -L858R/246-253* in HeLa cells demonstrates a decrease in mobility of EGFR-L858R relative to EGFR-WT, and that addition of the 246-253* mutation significantly increases mobility of the EGFR-L858R mutant. Shown are the cumulative probability plot **(C)** and extracted diffusion coefficients **(D)** * $p < 0.05$, n.s. not significant.